RDE Restorative Dentistry & Endodontics

Research Article

eISSN 2234-7666
Restor Dent Endod. 2025 August;50(3):e28
https://doi.org/10.5395/rde.2025.50.e28

Isolating design variables by assessing the impact of cross-section geometry on the mechanical performance of nickel-titanium rotary instruments: a comparative *in vitro* study

Anne Rafaella Tenório Vieira[1,*], Guilherme Ferreira da Silva[1], Emmanuel João Nogueira Leal da Silva[2,3], Rodrigo Ricci Vivan[1], João Vitor Oliveira de Amorim[1], Thaine Oliveira Lima[1], Raimundo Sales de Oliveira Neto[1], Marco Antonio Hungaro Duarte[1], Murilo Priori Alcalde[1]

[1]Department of Operative Dentistry, Endodontics, and Dental Materials, Bauru School of Dentistry, University of São Paulo – USP, Bauru, Brazil
[2]Department of Endodontics, School of Dentistry, State University of Rio de Janeiro (UERJ), Rio de Janeiro, Brazil
[3]Department of Endodontics, Grande Rio University (UNIGRANRIO), Rio de Janeiro, Brazil

ABSTRACT

Objectives: This study aimed to assess the effect of cross-section geometry on the mechanical properties of nickel-titanium (NiTi) instruments by comparing two instruments with identical tip size, taper, and thermal treatment but differing in cross-section design.

Methods: One hundred four NiTi rotary instruments, being S-shaped and triangular cross-section, manufactured with Blueish thermal treatment, were tested ($n = 52$ per group). Differential scanning calorimetry was employed, and the metal mass volume and cross-section area were assessed. The cyclic fatigue, torsional, and bending resistance tests were assessed. Data were analyzed using the Kolmogorov-Smirnov and Student *t*-tests, and the level of significance was set at 5%.

Results: The instruments exhibited similar start and finish temperatures of phase transformation. The S-shaped instruments had significantly lower metal mass volume and cross-sectional area ($p < 0.05$). S-shaped instruments demonstrated superior cyclic fatigue resistance, greater angular deflection, and lower bending stiffness ($p < 0.05$).

Conclusions: Cross-section geometry significantly influences the mechanical properties of NiTi rotary instruments.

Keywords: Endodontics; Fatigue; Mechanical tests; Nitinol

INTRODUCTION

The introduction of nickel-titanium (NiTi) rotary instruments has transformed endodontic practice, improving the efficiency and predictability of root canal shaping while reducing the risk of procedural errors [1]. Com-

Received: March 29, 2025 **Revised:** May 17, 2025 **Accepted:** June 2, 2025

Citation
Vieira ART, Silva GF, Silva EJNL, Vivan RR, Amorim JVO, Lima TO, Oliveira Neto RS, Duarte MAH, Alcalde MP. Isolating design variables by assessing the impact of cross-section geometry on the mechanical performance of nickel-titanium rotary instruments: a comparative *in vitro* study. Restor Dent Endod 2025;50(3):e28.

***Correspondence to**
Anne Rafaella Tenório Vieira, DDS
Department of Operative Dentistry, Endodontics, and Dental Materials, Bauru School of Dentistry, University of São Paulo – USP, Alameda Octávio Pinheiro Brisolla, 9-75, Vila Universitária, Bauru, SP 17012-901, Brazil
Email: annerft@gmail.com

pared to stainless-steel instruments, NiTi files exhibit superior flexibility, allowing for better canal centering and adaptation to complex root anatomies [2,3]. Furthermore, NiTi instruments combine optimal cutting efficiency and enhanced cyclic fatigue resistance, resulting in both safer and more effective root canal preparations [4,5]. However, despite these advancements, NiTi instruments remain susceptible to mechanical failure, particularly in anatomically complex canals where increased torsional stress and cyclic fatigue can lead to fracture [3]. Instrument separation during treatment disrupts root canal debridement and disinfection, potentially compromising overall treatment outcomes [6].

Given the risk of mechanical failure, ongoing research has focused on optimizing the design and metallurgical properties of endodontic instruments to enhance both performance and safety [3]. Manufacturers have introduced several modifications, including variations in cross-section geometry, pitch number, core diameter, taper, and thermal treatment of the NiTi alloy [3,5,7]. Among these factors, cross-section geometry plays a critical role in determining mechanical behavior. However, its specific influence remains underexplored, particularly in studies with well-controlled and methodologically sound designs. Along with tip design and taper, cross-section geometry significantly affects instrument stiffness by determining metal mass distribution, polar moment of inertia, and overall resistance to deformation [7,8]. In turn, stiffness is a key determinant of clinical performance, influencing cutting efficiency, stress distribution along the instrument, and shaping ability within the root canal system [3,5,7,8]. Given these considerations, clinicians must critically evaluate how different design features influence instrument performance to optimize their selection based on specific clinical needs [3,7].

Studies using finite element analysis suggest that triangular-based cross-sections, such as convex and triple-helix designs, may promote better stress distribution and lower stress concentration compared to S-shaped cross-sections [9–11]. This characteristic is supposedly associated with improved safety of NiTi instruments during root canal preparation, particularly in curved canals [10]. Conversely, other laboratory studies have reported that S-shaped cross-sections provide greater flexibility [12,13], improved flexural properties, and better centering ability compared to triangular-based designs [14,15]. These conflicting findings may stem from variations in experimental methodologies and differences in additional design features among commercially available NiTi instruments. Furthermore, finite element analysis has inherent limitations, as its accuracy depends on the material properties assigned to the virtual model and often fails to account for clinically relevant factors such as surface finish, microdefects, and manufacturing inconsistencies [16].

Understanding the influence of cross-section geometry on the mechanical properties of NiTi rotary instruments is essential for optimizing their clinical performance and ensuring predictable outcomes. To accurately assess this impact, cross-section geometry must be isolated as the only variable, ensuring that differences in mechanical behavior are not confounded by factors such as tip size, taper, or thermal treatment. Therefore, this study aimed to evaluate the influence of cross-section geometry on the mechanical properties of NiTi instruments by comparing two instruments with identical tip size, taper, and thermal treatment but differing in cross-section design. The null hypothesis states that cross-section geometry has no significant effect on the cyclic fatigue resistance, torsional resistance, or bending properties of the tested instruments.

METHODS

Sample size calculation and sample selection

Sample size calculation was performed using G*Power v3.1 software (Heinrich Heine University of Düsseldorf, Düsseldorf, Germany). The sample size estimation was based on preliminary results obtained from five initial tests. An alpha error of 0.05 and a statistical power of 80% were considered. The effect sizes used were: 11.1 for time to fracture, 4.4 for maximum torque, 6.9 for maximum rotation angle, and 1.9 for bending strength. The required sample sizes were determined as 2, 3, 3, and 6, respectively. To ensure robust statistical analysis, a final sample size of 10 instruments per group was selected.

A total of 104 rotary NiTi instruments (n = 52 per group) with either an S-shaped or triangular cross-section were selected for analysis. All instruments had a tip

https://doi.org/10.5395/rde.2025.50.e28

size of 25, a 0.06 taper, and a length of 25 mm. They were manufactured using Blueish thermal treatment (Mk Life Medical and Dental Products, Porto Alegre, Brazil) and evaluated for their mechanical properties and metallurgical characteristics. Prior to testing, all instruments underwent microscopic inspection at 16× magnification with LED illumination (Carl Zeiss Microscopy, LLC, White Plains, NY, USA) to identify any significant defects, such as blade design irregularities or unwinding, that could disqualify them from the study. No defects were found, and all instruments were deemed suitable for inclusion.

Design assessment

Six instruments from each group were randomly selected for examination under a stereomicroscope (Opmi Pico, Carl Zeiss Surgical, Jena, Germany) using ImageJ software (ver. 1.50e; Laboratory of Optical and Computational Instrumentation, Madison, WI, USA) at 13.6× magnification [17]. The images were analyzed to assess the length of the active cutting blade, number of spirals, spirals per millimeter, and spiral direction. For illustrative purposes, the instruments were also photographed using a digital camera (Canon EOS 500D; Canon, Tokyo, Japan) paired with a 1:1 Macro Lens (IRIX 150 mm F/2.8; TH Swiss, Baar, Switzerland) to ensure high-resolution images with minimal distortion (Figure 1).

Differential scanning calorimetry

Differential scanning calorimetry (DSC) tests were performed to assess the phase transformation temperatures of the tested instruments, following the protocol described by Teves Cordova *et al.* [18]. This standardized approach ensures reliable measurement of phase transitions by monitoring heat flow variations as a function of temperature. Small fragments (3–5 mm in length, 7–12 mg in weight) were sectioned from the active blade of each instrument (n = 6 per group) and etched in a solution of 25% hydrofluoric acid, 45% nitric acid, and 30% distilled water for 2 minutes. After rinsing with distilled water, the specimens were placed in aluminum pans, with an empty pan serving as a control. The heat cycle lasted 45 minutes and consisted of the following stages:

- Isothermal hold at 25°C for 5 minutes;
- Heating to 150°C at a rate of 10°C/min, followed by a 2-minute isothermal hold;
- Cooling to –30°C at 10°C/min, followed by another 2-minute isothermal hold;
- Reheating to 150°C at 10°C/min, with a final 2-minute isothermal hold;
- Final cooling to 25°C.

DSC analyses were conducted using the DSC Stare 1 system (DSC 204 F1 Phoenix; Netzsch-Gerätebau GmbH, Selb, Germany). The resulting phase transformation temperatures were processed with Netzsch Proteus Thermal Analysis software (Netzsch-Gerätebau GmbH). To ensure reproducibility, each test was performed twice per group, and results were compared for consistency.

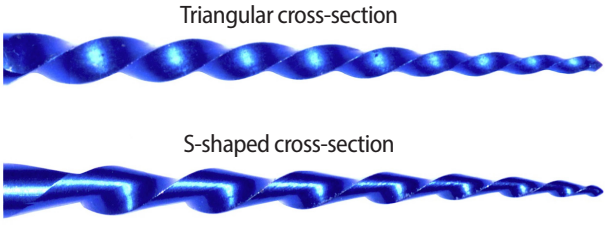

Figure 1. Macroscopic images of the instruments tested with triangular cross-section (top) and S-shaped cross-section (bottom).

Metal mass volume and cross-sectional area analysis

Twenty rotary NiTi instruments (n = 10 per group) with either an S-shaped or triangular cross-section were analyzed. Metal mass volume (mm^3) and cross-sectional area (μm^2) were assessed using micro-computed tomography (micro-CT) (Skyscan 1174v2; Bruker Belgium N.V., Kontich, Belgium), following a previously described methodology [19]. Micro-CT imaging was performed using the following parameters: 50 kV, 800 µA, 360° rotation, isotropic resolution of 14.1 µm, and a 0.5 mm-thick aluminum filter. The acquired images were reconstructed into cross-sectional slices perpendicular to the instrument's long axis using dedicated software (NRecon ver. 1.6.3, Bruker Belgium N.V.), allowing both two-dimensional (2D) and three-dimensional (3D) analyses. In the 3D analysis, metal mass volume was measured from the instrument tip to the 3rd and 5th mm (Figure 2A). For 2D analysis, reconstructed cross-section slices provided a topographic view at 3 and 5 mm from the tip, where the cross-section area (μm^2) was quantified for

comparison (Figure 2B).

Mechanical tests

Cyclic fatigue test was performed at body temperature (35°C ± 1°C) [19]. To maintain stable thermal conditions, the cyclic fatigue device was submerged in a histology water bath (Leica HI1210; Leica Biosystems, Milton Keynes, UK) filled with distilled water, with continuous temperature monitoring. The instruments were mounted on a 6:1 reduction handpiece (Sirona Dental Systems GmbH, Bensheim, Germany) and driven by a torque-controlled motor set to the RECIPROC ALL mode (VDW Silver; VDW GmbH, Munich, Germany). Instruments operated at 400 revolutions per minute (RPM) with a torque of 2 N•cm and were tested in a static position within an artificial stainless-steel canal with a 5-mm radius and a 60° curvature [19]. Fracture occurrence was identified through visual and auditory cues, and the time to fracture (in seconds) was recorded using a digital chronometer. The number of cycles to failure (NCF) was calculated as: NCF = (time to failure in seconds × RPM) / 60.

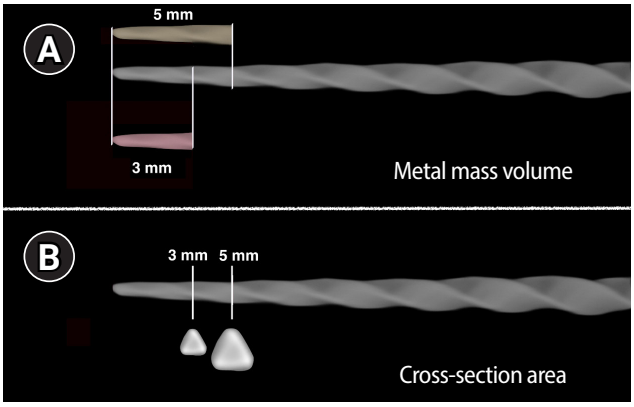

Figure 2. Representative images of micro-computed tomography analysis of metal mass volume and cross-section area. (A) The metal mass volume from the instrument tip to the 3 and 5 mm from the tip of the instrument. (B) The cross-section area was measured using the cross-section slices at 3 and 5 mm from the tip of the instrument.

Torsional strength (n = 10), assessed by measuring maximum torque (N•cm) and angle of rotation (°), along with bending resistance (n = 10), determined by maximum bending load (gf), were evaluated according to an international standard (ISO 3630-3631, 2008) and as previously reported [18,19].

Scanning electron microscopy

Fractured fragments from both cyclic fatigue and torsional tests were examined using scanning electron microscopy (SEM) (JSM-TLLOA; JEOL, Tokyo, Japan) to analyze the topographic features of the fracture surfaces. Images were acquired at 150× and 1,000× magnifications to assess characteristic failure patterns.

Statistical analysis

The evaluation of instrument design parameters, such as the number of blades and helical angle, was purely descriptive and therefore not subjected to statistical analysis. Similarly, the DSC analysis aimed to verify consistency in phase transformation temperatures (austenite start temperature [As] and austenite finish temperature [Af]) across the instruments treated with the Blueish thermal process, and as such, did not require inferential statistical testing.

The normality of the data from the mechanical tests (cyclic fatigue, torsional resistance, and bending), as well as the metal mass volume and cross-sectional area measurements, was confirmed using the Shapiro-Wilk test. Group comparisons were then performed using an independent Student t-test, with a significance level set at 5% (IBM SPSS ver. 22.0 for Windows; IBM Corp, Armonk, NY, USA).

RESULTS

Design assessment

The geometric design characteristics of the tested instruments are illustrated in Figure 1 and summarized in Table 1. The active blade length remained consistent at

Table 1. Geometric design characteristics of the assessed instruments

Instrument	Size/taper	Active blade length (mm)	Number of spirals	Spirals/mm	Helical angle (º)
S-Shaped	25/0.06	16	8	0.50	35.1
Triangular	25/0.06	16	9	0.56	25.4

https://doi.org/10.5395/rde.2025.50.e28

16 mm for both cross-section designs. Variations were observed in the number of spirals, with the S-shaped cross-section presenting eight spirals and the triangular cross-section exhibiting nine spirals. When adjusted for length, the number of spirals per millimeter was 0.56 for the S-shaped cross-section and 0.50 for the triangular cross-section. Additionally, the helical angle differed considerably between the groups, with the S-shaped cross-section displaying the highest mean helical angle (35.1°), while the triangular cross-section had the lowest mean helical angle (25.4°).

Differential scanning calorimetry analysis

The DSC analysis determined the As and Af temperatures of both tested instruments, representing the start (As) and finish (Af) points of the austenitic phase transformation. Both instruments exhibited comparable transformation temperatures, indicating similar thermal behavior under the Blueish thermal treatment. The S-shaped cross-section instruments had an As of 37.2°C and an Af of 41.8°C, while the triangular cross-section instruments presented an As of 36.9°C and an Af of 41.6°C. These findings indicate that both instruments maintained comparable phase transformation characteristics under the Blueish thermal treatment (Figure 3).

Cross-sectional area and metal mass volume

The results of the cross-sectional area (μm^2) and metal mass volume (mm^3) analyses are presented in Table 2. The S-shaped cross-section instruments exhibited a significantly lower metal mass volume at both 3 mm and 5 mm from the instrument's tip compared to the triangular cross-section instruments ($p < 0.05$). Similarly, the cross-sectional area of the S-shaped instruments was significantly smaller than triangular cross-sectional instruments ($p < 0.05$).

Mechanical tests

The results of cyclic fatigue, torsional resistance, and bending resistance tests are summarized in Table 3. The S-shaped cross-section instruments demonstrated significantly higher time to failure, NCF, and angular deflection compared to the triangular cross-section instruments ($p < 0.05$). Conversely, the triangular cross-section instruments exhibited higher torque and bending resistance (less flexibility) than the S-shaped cross-section instruments ($p < 0.05$).

Scanning electron microscopy evaluation

SEM analysis of the fractured surfaces revealed characteristic features of cyclic fatigue and torsional failure in

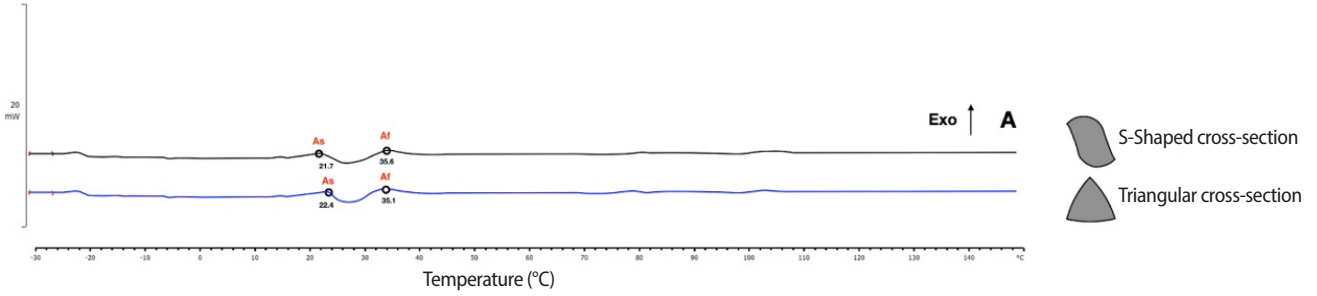

Figure 3. The differential scanning calorimetry (DSC) charts display the heating curves of the S-shaped and triangular cross-section instruments. The charts highlight the austenite start (As) temperature (on the left) and the austenite finish (Af) temperature (on the right) for each instrument. Overall, the DSC analysis revealed no significant difference in the phase transformation between the tested instruments.

Table 2. Metal mass volume and cross-section area measured at 3 mm and 5 mm from the tip of the tested instruments

Instrument	Metal mass volume (mm^3)		Cross-section area (μm^2)	
	3 mm	5 mm	3 mm	5 mm
S-Shaped	0.13 ± 0.01^A	0.36 ± 0.02^A	80.1 ± 0.3^A	122.4 ± 0.1^A
Triangular	0.18 ± 0.01^B	0.41 ± 0.02^B	91.7 ± 0.3^B	142.1 ± 0.1^B

Values are presented as mean ± standard deviation.
Different superscript letters in the same column indicate statistical differences between groups ($p < 0.05$).

Table 3. Cyclic fatigue[a], torsional[b], and bending[c] resistance of the tested instruments

Instrument	Cyclic		Torsional		Bending 60°
	Time (sec)	NCF	Torque (N.cm)	Angular deflection (°)	Force (g/f)
S-Shaped	475 ± 26^{A}	3165 ± 50^{A}	0.89 ± 0.07^{A}	467 ± 18^{A}	112 ± 20^{A}
Triangular	154 ± 31^{B}	1030 ± 40^{B}	1.27 ± 0.10^{B}	347 ± 15^{B}	156 ± 24^{B}

Values are presented as mean ± standard deviation.
Different superscript letters in the same column indicate statistical differences between groups ($p < 0.05$).
[a]Time to fracture and number of cycles to failure (NCF); [b]maximum torque and angular deflection; [c]force at 60° deflection.

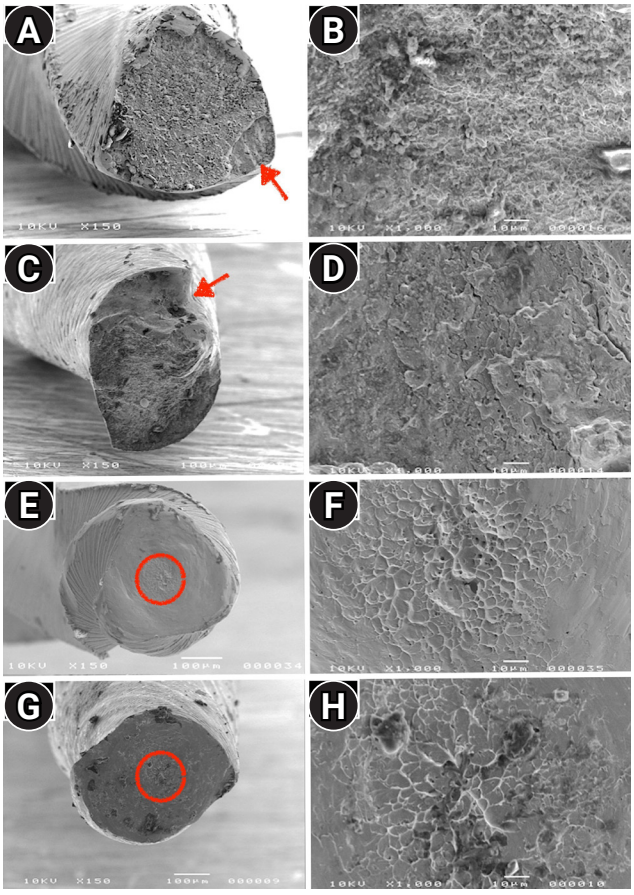

Figure 4. Scanning electron microscopy images of the fractured surfaces of the instrument fragments after cyclic (A–D) and torsional fatigue (E–H) testing, at 150× and 1,000× magnification. The cyclic fatigue images of the triangular (A, B) and S-shaped cross-section (C, D) show numerous dimples, characteristic of ductile fracture. The red arrows indicate the point of crack initiation. The torsional fatigue images of the triangular (E, F) and S-shaped cross-section (G, H) reveal concentric abrasion marks and skewed dimples near the center of rotation, which are typical features of torsional failure. The red circles indicate the point of concentric abrasion marks and skewed dimples.

both instrument groups. SEM images of the fractured surfaces of the instrument fragments after cyclic (Figure 4A–D) and torsional fatigue (Figure 4E–H) testing. The cyclic fatigue images of the triangular (Figure 4A, B) and S-shaped cross-section (Figure 4C, D) show a crack initiation area followed by numerous dimples, characteristic of ductile fracture. The torsional fatigue images of the triangular (Figure 4E, F) and S-shaped cross-section (Figure 4G, H) reveal concentric abrasion marks and fibrous dimples near the center of rotation, which are typical features of torsional failure.

DISCUSSION

The present study evaluated the influence of cross-section geometry on the mechanical performance of NiTi rotary instruments while eliminating confounding variables by maintaining identical tip size, taper, and thermal treatment. To assess how cross-section design affects mechanical behavior, three critical parameters were analyzed: cyclic fatigue resistance, torsional strength, and bending resistance. Previous studies have established that instrument design—including cross-section geometry, taper, and core diameter—directly impacts mechanical properties and fatigue resistance [3,7,8,13,14]. However, most of these studies compared instruments from different manufacturers or included additional design variations, making it difficult to isolate the specific effect of cross-section geometry [8,12–15]. To overcome this limitation, the present study was meticulously designed to ensure that all tested instruments underwent the same Blueish thermal treatment and shared identical tip size and taper. By standardizing these key parameters, this study provides a unique opportunity to assess the isolated effect of cross-section geometry on mechanical performance,

https://doi.org/10.5395/rde.2025.50.e28

free from extraneous variables. This methodological rigor minimizes bias, enhances the validity of the findings, and offers a precise evaluation of how cross-section geometry influences NiTi instrument behavior in endodontic applications.

In this study, DSC analysis was performed to confirm that both instruments underwent the same thermal treatment. Although both were produced by the same manufacturer and exhibited the characteristic Blueish coloration, DSC testing was essential because the machining process itself can alter the crystallographic structure of NiTi alloys. The results demonstrated that the As and Af temperatures were similar for both cross-section designs (Figure 2), confirming that no significant structural modifications occurred due to processing. At room temperature (20°C), both instruments remained in the martensitic phase, transitioning to an austenitic structure at body temperature (36°C). These findings were critical in ensuring that any differences in mechanical performance could be attributed exclusively to cross-section geometry, as no significant variations in thermal behavior or phase transformation were detected.

Prior to the mechanical tests, the instruments were scanned using micro-CT to perform both 2D (cross-sectional area, μm^2) and 3D (metal mass volume, mm^3) analyses at 3 mm and 5 mm from the instrument tip. This analysis allowed for a direct correlation between cross-section geometry and mechanical performance during testing. The results demonstrated that S-shaped cross-section instruments exhibited significantly lower metal mass volume and cross-section area compared to triangular cross-section instruments at both analyzed levels ($p < 0.05$) (Table 2). These findings confirm that cross-section geometry directly influences metal mass distribution, a key factor in determining flexibility, fatigue resistance, and overall mechanical behavior. Such an analysis is crucial for understanding how geometric modifications impact instrument performance, emphasizing the role of design parameters in shaping mechanical properties and their potential clinical implications [3,16].

During root canal preparation, NiTi instruments are subjected to both cyclic and torsional stresses, which are recognized as the primary causes of instrument failure [4,20]. Cyclic fatigue occurs due to repeated flexion of the instrument within curved canals, while torsional failure results from binding within narrow canal spaces, leading to excessive torque generation [20]. Laboratory tests assessing cyclic fatigue and torsional resistance serve as key indicators of an instrument's ability to withstand these failure modes under clinical conditions. Additionally, bending resistance tests are used to evaluate instrument flexibility, a crucial property that enhances centering ability in curved canals [3,16] and plays a significant role in determining fatigue resistance. However, while these laboratory tests provide valuable insights into mechanical behavior, their direct translation to clinical performance should be interpreted with caution, as *in vivo* conditions introduce additional variables that may influence instrument performance.

The mechanical test results demonstrated that S-shaped cross-section instruments exhibited superior performance in several parameters, including time to fracture, NCF, and angular deflection ($p < 0.05$) (Table 3). In contrast, the triangular cross-section instruments displayed significantly higher torque to fracture ($p < 0.05$) (Table 3). Given the statistically significant differences observed between the tested instruments, the null hypothesis was rejected. These findings confirm that cross-section geometry plays a critical role in determining the mechanical properties of NiTi instruments, as previously reported [7,8,12–15]. The lower metal mass volume and cross-section are of the S-shaped cross-section contributed to greater flexibility, which in turn explains its superior cyclic fatigue resistance, lower bending stiffness, and greater angular deflection in torsional tests. The combination of enhanced cyclic fatigue resistance and reduced bending stiffness may help reduce the risk of instrument fracture while improving root canal preservation, particularly in curved canals [3,7,8]. Additionally, the higher angular deflection observed in S-shaped instruments could provide clinicians with an early indication of plastic deformation, signaling an imminent risk of fracture [21]. The results of this study align with those reported by Kim *et al.* [12], which demonstrated that instruments with an S-shaped cross-section exhibit greater flexibility compared to those with a triangular cross-section. This finding confirms that S-shaped cross-sections tend to offer greater flexibility than triangular designs, as reported by pre-

vious authors [13–15]. Conversely, the higher torsional strength of the triangular cross-section is a relevant factor in the preparation of constricted canals, where instruments are subjected to greater torsional loads [21]. The highest torque to fracture of triangular cross-section instruments demonstrated in this study aligns with previous studies that reported higher torque to fracture than S-shaped cross-section instruments [12–15]. Therefore, the greatest torsional resistance of triangular cross-sections may offer resistance under high torsional stress, making them potentially more suitable for challenging canal anatomies requiring greater torque application, decreasing the risks of torsional failure. However, S-shaped instruments tend to exhibit greater cutting efficiency and an improved ability to reach the working length, which could enhance their performance even in constricted canals. Their sharper cutting edges and reduced metal mass may facilitate apical progression with less screwing-in effect, potentially minimizing the risk of excessive torsional stress. These factors suggest that, despite their lower torsional strength, S-shaped instruments could still perform effectively in narrow canals. Future studies with similar methodological designs should evaluate additional conditions to further clarify these findings and their impact on clinical outcomes.

This study has certain limitations that should be acknowledged. As a laboratory-based investigation, the experimental conditions do not fully replicate the complex *in vivo* environment, where factors such as dentin hardness, anatomical variations, and irrigation dynamics may influence instrument performance. Additionally, while this study successfully isolated cross-section geometry as the only variable, further research should explore its interaction with other parameters, such as kinematics and surface treatments, to provide a more comprehensive understanding of instrument behavior. Moreover, this study focused on specific mechanical properties, and additional tests could further clarify the clinical implications of cross-section geometry. Despite these limitations, the study's controlled methodology represents a key strength, allowing for an accurate assessment of how cross-section design influences mechanical properties. These findings have important clinical implications, such as instrument flexibility, fatigue resistance, and torsional strength are critical factors in preventing procedural errors and optimizing root canal preparation. Additionally, the use of complementary methodologies provided a more comprehensive dataset, enabling a deeper understanding of the relationship between instrument geometry and mechanical performance. By integrating different analytical techniques, this study moves beyond speculative assumptions, offering a more objective, data-driven interpretation of the findings. This approach strengthens the reliability of the results, reinforcing that cross-section geometry plays a decisive role in determining instrument behavior. Future studies should incorporate micro-CT analysis to evaluate the shaping ability of these instruments in anatomically complex canals, further validating their clinical applicability and guiding endodontists in selecting instruments that balance safety, efficiency, and durability.

CONCLUSIONS

Cross-section geometry significantly influences the mechanical properties of NiTi rotary instruments. The S-shaped cross-section exhibited lower metal mass volume, which contributed to greater flexibility and higher cyclic fatigue resistance. In contrast, the triangular cross-section demonstrated superior torque to fracture.

CONFLICT OF INTEREST

Emmanuel João Nogueira Leal da Silva is an Associate Editor of *Restorative Dentistry and Endodontics* and was not involved in the peer-review or editorial process of this article. The authors declare no other conflicts of interest.

FUNDING/SUPPORT

The authors have no financial relationships relevant to this article to disclose.

AUTHOR CONTRIBUTIONS

Conceptualization: Vieira ART, Silva EJNL, Alcalde MP, Vivan RR, Duarte MAH. Data curation, Validation: all authors. Formal analysis: Alcalde MP, Duarte MAH, Silva EJNL. Funding acquisition: Alcalde MP. Investigation: Vieira ART, Silva EJNL, Amorim JVO, Lima TO, Oliveira Neto RS, Alcalde MP. Methodology: Silva EJNL, Silva GF, Duarte MAH, Vivan RR, Alcalde MP. Project administration: Vieira ART, Silva EJNL, Alcalde MP. Resources, Supervision, Software: Silva EJNL, Alcalde MP. Writing - original draft: Vieira ART, Silva EJNL, Alcalde MP. Writing - review & editing: Alcalde MP, Silva EJNL. All authors read and approved the final manuscript.

https://doi.org/10.5395/rde.2025.50.e28

DATA SHARING STATEMENT

The datasets are not publicly available but are available from the corresponding author upon reasonable request.

REFERENCES

1. Bürklein S, Arias A. Effectiveness of root canal instrumentation for the treatment of apical periodontitis: a systematic review and meta-analysis. Int Endod J 2023;56 Suppl 3:395-421.
2. Zupanc J, Vahdat-Pajouh N, Schäfer E. New thermomechanically treated NiTi alloys : a review. Int Endod J 2018;51:1088-1103.
3. Silva EJ, Martins JN, Ajuz N, Vieira VT, Pinto R, Marques D, *et al*. Multimethod analysis of a novel multi-coloured heat-treated nickel-titanium rotary system: design, metallurgy, mechanical properties, and shaping ability. J Endod 2024;50:1622-1633.
4. Gavini G, Santos MD, Caldeira CL, Machado ME, Freire LG, Iglecias EF, *et al*. Nickel-titanium instruments in endodontics: a concise review of the state of the art. Braz Oral Res 2018;32(Suppl 1):e67.
5. De-Deus G, Silva EJ, Vieira VT, Belladonna FG, Elias CN, Plotino G, *et al*. Blue thermomechanical treatment optimizes fatigue resistance and flexibility of the Reciproc files. J Endod 2017;43:462-466.
6. Gulabivala K, Ng YL. Factors that affect the outcomes of root canal treatment and retreatment: a reframing of the principles. Int Endod J 2023;56 Suppl 2:82-115.
7. Zhang EW, Cheung GS, Zheng YF. Influence of cross-sectional design and dimension on mechanical behavior of nickel-titanium instruments under torsion and bending: a numerical analysis. J Endod 2010;36:1394-1398.
8. Bürklein S, Zupanc L, Donnermeyer D, Tegtmeyer K, Schäfer E. Effect of core mass and alloy on cyclic fatigue resistance of different nickel-titanium endodontic instruments in matching artificial canals. Materials (Basel) 2021;14:5734.
9. Gharechahi M, Moezzi S, Karimpour S. Comparative analysis of stress distribution through finite-element models of 3 NiTi endodontic instruments while operating in different canal types. J Dent (Shiraz) 2023;24:60-65.
10. Akkoç Hİ, Keskin C, Aslantaş K. Dynamic analysis of a NiTi rotary file by using finite element analysis: effect of cross-section and pitch length. Aust Endod J 2024;50:649-657.
11. Xu X, Eng M, Zheng Y, Eng D. Comparative study of torsional and bending properties for six models of nickel-titanium root canal instruments with different cross-sections. J Endod 2006;32:372-375.
12. Kim HC, Kwak SW, Cheung GS, Ko DH, Chung SM, Lee W. Cyclic fatigue and torsional resistance of two new nickel-titanium instruments used in reciprocation motion: Reciproc versus WaveOne. J Endod 2012;38:541-544.
13. Faus-Llácer V, Hamoud-Kharrat N, Marhuenda Ramos MT, Faus-Matoses I, Zubizarreta-Macho Á, Ruiz Sánchez C, *et al*. Influence of the geometrical cross-section design on the dynamic cyclic fatigue resistance of NiTi endodontic rotary files: an in vitro study. J Clin Med 2021;10:4713.
14. Donnermeyer D, Viedenz A, Schäfer E, Bürklein S. Impact of new cross-sectional designs on the shaping ability of rotary NiTi instruments in S-shaped canals. Odontology 2020;108:174-179.
15. Maia Filho EM, Dos Reis Santos RM, Lima DM, da Silva Pereira SM, Soares JA, de Jesus Tavarez RR, *et al*. Shaping ability of ProTaper Next, WaveOne, and Reciproc in simulated root canals. J Contemp Dent Pract 2016;17:902-906.
16. Martins JN, Martins RF, Braz Fernandes FM, Silva EJ. What meaningful information are the instruments mechanical testing giving us? A comprehensive review. J Endod 2022;48:985-1004.
17. Silva EJ, Martins JN, Ajuz NC, Dos Santos Antunes H, Vieira VT, Braz-Fernandes FM, *et al*. Design, metallurgy, mechanical properties, and shaping ability of 3 heat-treated reciprocating systems: a multimethod investigation. Clin Oral Investig 2023;27:2427-2436.
18. Teves Cordova AV, Alcalde MP, Vivan RR, Zevallos Quiroz CA, Guzmán HP, Calefi PS, *et al*. Impact of metallurgical features on the cyclic and torsional properties of five reciprocating instruments manufactured with blue thermal treatment. Microsc Res Tech 2025;88:1979-1988.
19. Alcalde M, Duarte MA, Amoroso Silva PA, Souza Calefi PH, Silva E, Duque J, *et al*. Mechanical properties of ProTaper Gold, EdgeTaper Platinum, Flex Gold and Pro-T Rotary Systems. Eur Endod J 2020;5:205-211.
20. McGuigan MB, Louca C, Duncan HF. Endodontic instrument fracture: causes and prevention. Br Dent J 2013;214:341-348.
21. Ninan E, Berzins DW. Torsion and bending properties of shape memory and superelastic nickel-titanium rotary instruments. J Endod 2013;39:101-104.